Pergamon

Tetrahedron 56 (2000) 7027–7040

TETRAHEDRON

Adenine-Thymine Base Pair Recognition by an Anthryl Probe from the DNA Minor Groove

Challa V. Kumar,* Emma H. A. Punzalan† and Willy B. Tan

Department of Chemistry, University of Connecticut, Storrs, CT 06269-3060, USA

Received 20 December 1999; revised 5 February 2000; accepted 7 February 2000

Abstract—Synthesis and DNA binding properties of geometric isomers, 9(3-aminopropyl)anthracene (**APAC**) and 9(*N*-ethyl)aminomethyl anthracene (**N-Et-AMAC**) are reported here. The aminopropyl side chain of **APAC** can position the amino function in the DNA grooves for hydrogen bonding with the heterocyclic bases. In contrast, the *N*-ethyl-aminomethyl side chain of **N-Et-AMAC** is too short to make contacts in the grooves. The DNA binding properties are examined using absorption, fluorescence, circular dichroism (CD), singlet–singlet energy transfer, and DNA melting experiments. In addition to calf thymus DNA (CTDNA), we examined poly(dA-dT), poly(dG-dC), poly(dA)-poly(dT), and poly(dI-dC). The spectroscopic and thermal studies indicate intercalation of the anthryl probes into the helix. The binding properties, however, depended on the side chain as well as the DNA sequence. The binding of **APAC** to poly(dA-dT) is preferred 3.4 times better over poly(dG-dC) while binding of **N-Et-AMAC**, the geometric isomer of **APAC**, is nearly the same with all the DNA polymers examined. Hydrogen bonding of the probe side chain from the minor groove of the helix is tested by using inosine-cytosine sequences. Consistent with the above data, **APAC** binds to poly(dI-dC) with binding constants similar to that of poly(dA-dT) sequences. Thus, both chemical and biochemical methods are used to test the hydrogen bonding of the probe side chains with the helix. The DNA sequence discrimination observed here clearly indicates the position of the amino function on the side chain plays an important role in DNA sequence recognition. The helix melting temperature of CTDNA is increased from 70°C to 80 and 82°C by **APAC** and **N-Et-AMAC**, respectively, indicating the helix stabilization upon intercalation of the probes. Intercalation is also supported by the CD spectra of the probe-DNA complexes. The probes are achiral and binding to the helix leads to induced CD spectra in the 300–400 nm region, away from the DNA absorption bands. The positive CD bands observed indicate intercalation of the anthryl chromophore with its long axis perpendicular to the base-pair dyad axis. Fluorescence polarization data clearly support intercalation of both probes into the above sequences, including poly(dI-dC), except that no polarization was observed with **APAC** bound to poly(dG-dC). This result is consistent with preferential binding of **APAC** to AT sites over GC sites and efficient quenching of anthryl emission at GC sites. Excitation into the DNA absorption bands results in sensitized emission from the anthryl probes and the efficiency of energy transfer depends upon the sequence. While AT sites sensitize anthryl emission efficiently, no sensitization was noted for GC sequences. These data clearly show that GC and IC sequences can be readily distinguished, in addition to AT sequences, by monitoring the sensitized emission from the anthryl probes. Thus, a comparison of the binding properties of **APAC** and **N-Et-AMAC** as well as a comparison of the binding properties of each probe as a function of DNA sequence clearly indicate the ability of the propyl side chain on the intercalator to position the hydrogen bonding group in the minor groove of the helix. Both probes can induce photochemical DNA strand damage that results in sugar-phosphate backbone cleavage. The photocleavage of the supercoiled DNA results in nicked circular DNA with little or no linear DNA suggesting that single stranded cleavage predominates. Most likely, the O2 of thymine in AT bases and O2 of cytosine in IC sequences interact with the aminopropyl side chain of **APAC** and this interaction provides the basis for the DNA nucleobase recognition by the small molecules.

Introduction

The design of small molecules that can bind to specific sequences of DNA has attracted much attention due to their potential use in the development of new anticancer agents[1] and in site-specific manipulation of DNA.[2] One approach for the design has been to attach DNA binding molecules to natural recognition elements such as oligonucleotides, peptides or polysaccharides to achieve specificity.[3] Another approach has been to decorate the DNA binding ligands with functional groups that could make specific contacts with the double helix and serve as recognition elements.[4] The latter approach was inspired by the fact that several natural antibiotics,[5] and heterocyclic cations[6] bind to specific DNA sequences with high affinities. Therefore, DNA binding studies with small molecules of well defined topology, structure and conformation are valuable in understanding the basis for DNA sequence recognition by small molecules.[7]

Several bifunctional DNA binding agents (Scheme 1) are designed, synthesized and their DNA binding properties

Keywords: circular dichroism; anthryl probe; photocleavage DNA.

* Corresponding author. Tel.: +1-860-486-3213; fax: +1-860-486-2981; e-mail: cvkumar@nucleus.chem.uconn.edu

† Current address: United Laboratories, Inc., Quality Assurance and Chemistry Division, No. 66 United Street, Mandaluyong City, Philippines.

0040–4020/00/$ - see front matter
PII: S0040-4020(00)00526-3

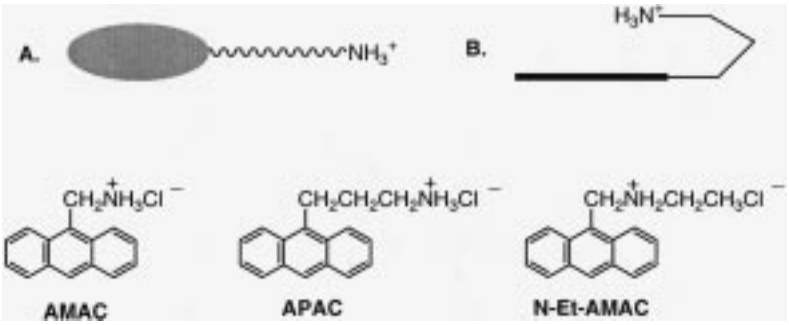

Scheme 1. The design of anthryl probes and their structures.

have been tested in our laboratory. A planar hydrophobic fluorescent moiety, anthryl, capable of intercalation is attached to a hydrophilic cationic function through an appropriate linker. While the planar anthryl moiety is expected to intercalate into the helix, the cationic function can provide favorable electrostatic interactions. Geometry permitting, the cationic ammonium group of the side chain can be positioned on the helix to hydrogen bond and serve as a recognition element. The linker connecting these two functionalities is varied, in the current studies, to test how the linker controls the DNA recognition properties of the anthryl probe. The anthryl chromophore is chosen for several reasons. The anthryl is a hydrophobic planar intercalator[8] and it absorbs in the 320–390 nm region, at much longer wavelengths than the nucleobases. The singlet excited state of the anthryl fluorophore is photoreactive and provides an opportunity to design photoreactions to induce DNA cleavage at the probe binding site.[9] Incorporation of spectroscopic, reactive, and recognition elements in a single ligand is the basis for the current design.

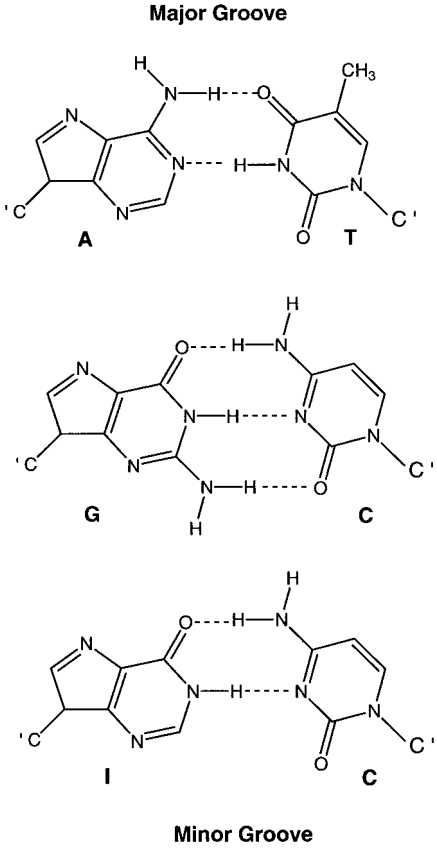

Scheme 2. Hydrogen binding sites in the grooves of AT, GC and IC base pairs. The major groove is above the base pair while the minor groove is below (as shown).

The length and flexibility of the linker connecting the hydrophobic and cationic functions is expected to be important in controlling the binding properties of the ligand. For example, 9-anthrylmethylammonium chloride (**AMAC**, Scheme 1) binds to DNA, with little or no sequence specificity.[8] Molecular modeling studies show that when the anthryl moiety is intercalated, a linker such as an ethyl or propyl can position the ammonium function on the helix for hydrogen bonding with the bases above or below the plane of intercalation (Scheme 1B). The pattern of hydrogen binding sites in the major and minor grooves of DNA is sensitive to the DNA sequence (Scheme 2) and this heterogeneity is exploited for DNA sequence recognition;[1–7] 3-(9-anthryl)propylammonium chloride (**APAC**), for example, is expected to hydrogen bond to AT sequences from the minor groove (Scheme 2), while such binding to GC sites is hindered. **APAC** is, therefore, expected to bind better to AT sites than to GC sites. Preference for binding to AT sites over the GC sites has been reported for anthracene derivatives with hydroxyl groups at the α position.[10,11] Hydrogen bonding of the hydroxyl with the O2 of thymine bridged by a water molecule was suggested to be a major factor in the preferred binding of these molecules to AT sequences.

The role of the side chain and the ammonium group in the binding behavior of **APAC** can be tested with *N*-ethyl-(9-anthryl)methylammonium chloride (**N-Et-AMAC**), the geometric isomer of **APAC**. Since the stereochemical details and the steric requirements of the side chains of **APAC** and **N-Et-AMAC** are nearly identical, the location of the ammonium group on the side chain and its influence on the overall DNA binding properties can be ascertained. The ammonium group in **N-Et-AMAC** is less likely to interact with the AT sites in contrast to what is predicted for **APAC**. This is because, the ammonium functionality in **N-Et-AMAC** is moved to the interior of the side chain. Therefore, a comparison of the DNA binding properties of **APAC**, and **N-Et-AMAC**, will illustrate the effect of the propyl side chain in **APAC** on its ability to discriminate between different DNA sequences.

Another way to examine hydrogen bonding in the minor or

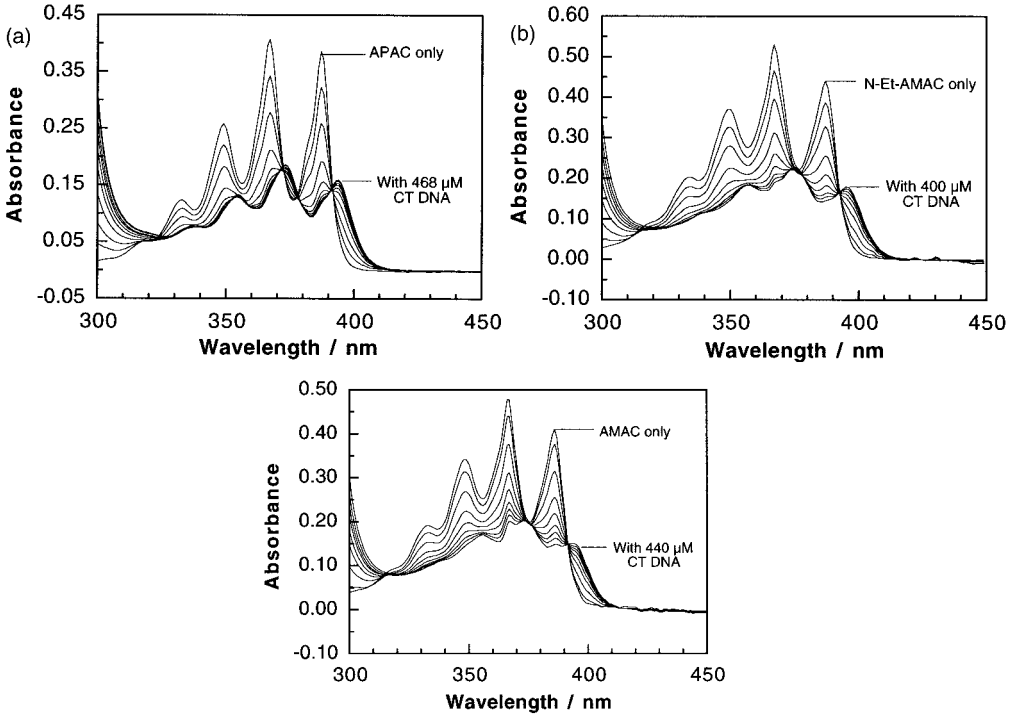

Figure 1. (a) Absorption spectra of **APAC** (48 μM) with increasing concentrations of CTDNA (0–468 μM). (b) Absorption spectra of **N-Et-AMAC** (95 μM) with increasing concentrations of CTDNA (0–400 μM). (c) Absorption spectra of **AMAC** (63 μM) with increasing concentrations of CTDNA (0–440 μM).

the major groove is to compare the binding properties of the above probes with GC and IC (inosine-cytosine) sequences. The locations of the hydrogen bonding functionalities in the minor groove of AT sequences is similar to that of IC sequences (Scheme 2), while the hydrogen bonding sites in the major groove of GC sequences are similar to that of IC sequences. Therefore, if hydrogen bonding in the minor groove leads to base recognition then the probes should bind to AT and IC sequences with nearly equal affinity but discriminate against GC sequences. Similarly, if the hydrogen bonding in the major groove is important then the binding affinities of the probes with GC and IC sequences are expected to be similar but discriminate against AT sequences. Thus, a comparison of the binding properties of **APAC** and **N-Et-AMAC** with GC, AT and IC sequences provides a simple way to test if hydrogen bonding in the grooves of DNA is a key factor for DNA base recognition by these molecules.

The DNA binding properties of **AMAC**, **APAC** and **N-Et-AMAC** are investigated using absorption, fluorescence, circular dichroism (CD), helix melting, and photochemical methods. Current results show that **APAC** prefers binding to alternating AT and IC sequences while no such base preference was observed for **N-Et-AMAC** or its analog, **AMAC**.

Results and Discussion

Spectroscopic, biophysical and photochemical methods have been used to ascertain the DNA binding features of two geometric isomers **APAC** and **N-Et-AMAC**. The position of the hydrogen bonding group in the side chain is varied in these anthryl probes to evaluate the role of the side chain in the DNA base recognition. A strong relationship between the structure of the probe and its base specificity was inferred from these data. At first, the binding properties of the probes with CTDNA are compared and then their dependence on the DNA sequence is presented.

Absorption spectral studies

The electronic absorption spectra of **APAC**, and **N-Et-AMAC** change dramatically upon binding to DNA. For example, strong hypochromism, extensive broadening and red shift of the vibronic bands of the anthryl chromophore are observed upon binding to DNA. The spectral changes are used to estimate the binding constants and to evaluate the sequence dependent binding of the anthryl probes.

The absorption spectra of **APAC** (48 μM) recorded in the presence of increasing amounts of calf thymus DNA (0–460 μM in bp) (Fig. 1a) show strong hypochromism. A small red shift of 6 nm and isosbestic points at 390 and 378 nm are evident. Broadening of the anthryl vibronic bands, and ~63% decrease in the absorption intensity (at 385 nm) are observed. These observations are similar to the earlier results obtained with **AMAC** and CTDNA,[8,12] although some differences are noteworthy. The vibronic bands of **APAC** are well resolved when the binding is nearly complete, and provide a sharp contrast to the extensively broadened bands observed with **N-Et-AMAC** and CTDNA (see below). Large hypochromism, and the red-shift in the absorption spectra indicate a strong electronic interaction between the anthryl moiety and the DNA bases.[13] No such interaction was observed in the presence of single stranded DNA, or when the helix was denatured. Since the strength of the interaction is inversely proportional to the cube of the

Table 1. The absorption spectral properties of **APAC** and **N-Et-AMAC** in the presence of CTDNA such as extinction coefficients at 365 nm, per cent hypochromism observed at 385 nm, and the binding constants

Probe	ϵ_{free} (M^{-1} cm^{-1})	ϵ_{bound} (M^{-1} cm^{-1})	% Hypochromism (385 nm)	K (M^{-1} in base pairs)
APAC	7830	3420±46	63±4	$1.4\pm0.1\times10^4$
N-Et-AMAC	4950	2310±169	62±4	$1.2\pm0.1\times10^4$

distance of separation between the chromophore and the DNA bases,[14] current results suggest that the anthryl chromophore of **APAC** is closely associated with the DNA bases.

Similar changes in the absorption spectrum of **N-Et-AMAC** (95 μM) are observed in the presence of calf thymus DNA (0–400 μM in bp) (Fig. 1b), but the spectral features are significantly broader when compared to those observed with **APAC**/CTDNA. For example, the peaks at 375 and 395 nm are separated by a valley of depth 29% of the average heights of the two peaks. The corresponding valley depth between the peaks at 373 and 393 nm in **APAC**/CTDNA spectrum was 45% of the average peak heights. Such broadening was also observed with **AMAC**/CTDNA (Fig. 1c). with a valley depth of 21%. Thus, the peaks of **N-Et-AMAC** and **AMAC** are perceptibly broader than those of **APAC**. The isosbestic points for **N-Et-AMAC** spectra are at 392 and 379 nm with ~62% decrease in the absorption at 385 nm (Table 1). The extensive broadening of the vibronic bands of **N-Et-AMAC** upon binding to DNA may indicate low selectivity. The structured absorption spectrum of **APAC**/CTDNA can be assigned to the discriminative binding of **APAC** to a subset of binding sites (discussed below), while **AMAC** and **N-Et-AMAC** are less selective. Binding of the probes to a polyanion such as sodium poly(styrene-4-sulphonate) did not result in such spectral changes.[15] Mere electrostatic binding of these cations to DNA, thus, does not result in significant broadening or hypochromism. The percent hypochromism and the extent of broadening depended on the probe structure, the DNA sequence, and ionic strength of the medium, suggesting that these changes are not due to simple ionic binding to the helix (Scheme 3A).

The absorption spectra of the probes, upon binding to the DNA, show a strong dependence on the DNA sequence (Fig. 2a–c for **AMAC**, **APAC**, and **N-Et-AMAC**, respectively). Typical spectra recorded at the highest DNA concentration are shown. **AMAC** spectra in the presence of poly(dI-dC) and poly(dA-dT) are virtually the same as that with CTDNA, but distinct from the spectrum obtained with poly(dA)-poly(dT) or poly(dG-dC) (not shown). The absorption spectra of **APAC** in the presence of poly(dA-dT) and poly(dI-dC) show hypochromism as well as bathochromic shifts but no shifts are evident with poly(dG-dC) or poly(dA)-poly(dT). Again, the vibronic bands of **APAC** are well separated with deep valleys between the peaks. Absorption spectra of **N-Et-AMAC** in the presence of various sequences are similar to those observed with **AMAC**. The spectral features vary with DNA sequence for **APAC** with considerable structure

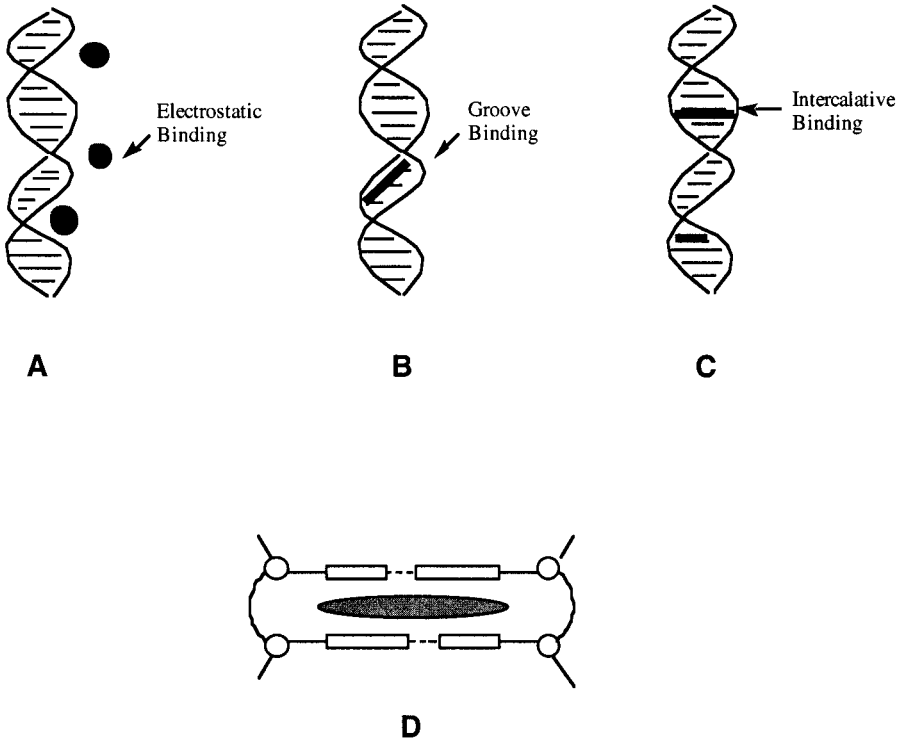

Scheme 3. Three distinct DNA binding modes for small ligands (A, B, C) and expanded view of the intercalation into the helix (D), the shaded oval represents the intercalator.

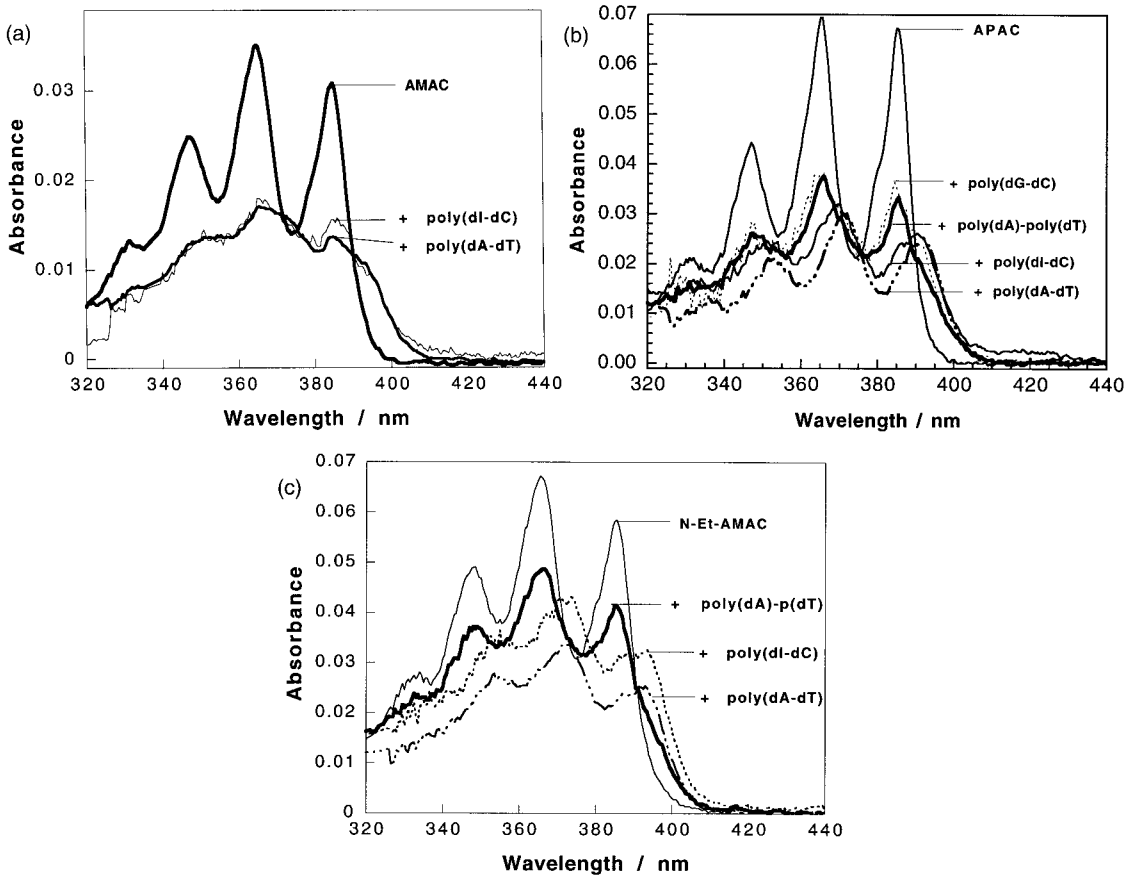

Figure 2. (a) Absorption spectra of **AMAC** (6 μM) in the presence of various DNA sequences (154 μM poly(dA-dT), 161 μM poly(dA)-poly(dT), and 141 μM poly(dI-dC)). (b) Absorption spectra of **APAC** (9.6 μM) in the presence of various DNA sequences (314 μM poly(dA-dT), 332 μM poly(dA)-poly(dT), 320 μM poly(dI-dC), and 347 μM poly(dG-dC)). (c) Absorption spectra of **N-Et-AMAC** (8.3 μM) in the presence of various DNA sequences (405 μM poly(dA-dT), 332 μM poly(dA)-poly(dT), and 320 μM poly(dI-dC)).

when compared to those for **AMAC** and **N-Et-AMAC**. One exception to the above generalization is poly(dA)-poly(dT). All three probes gave well resolved spectra with this polymer, and this result could be due to weak binding of the probes to this polymer or that these probes prefer groove binding into these helices (Scheme 3b) rather than intercalation. The spectral parameters extracted from these data are collected in Table 2.

Binding constants

The absorption spectral changes observed with **AMAC**, **APAC** and **N-Et-AMAC** are used to estimate their respective binding constants. The spectral data are plotted according to Eq. (1), and representative examples of the binding plots are shown in Fig. 3. The binding constants with CTDNA are $1.4\pm0.1\times10^4$ and $1.2\pm0.1\times10^4$ M^{-1} (DNA base pairs) for **APAC** and **N-Et-AMAC**, respectively (Table 3) and these values are comparable to that of **AMAC** ($1.5\pm0.5\times10^4$). The binding constants are nearly the same with CTDNA for the three probes, within our experimental error. These binding constants are comparable to those of the typical intercalating agents reported in the literature.[16]

Table 2. The extinction coefficients of **APAC** and **N-Et-AMAC** at 365 nm (M^{-1} cm^{-1}) as a function of the DNA sequence

DNA	APAC	N-Et-AMAC
Poly (dA-dT)	2080±150	1470±60
Poly (dA)-Poly(dT)	3480±5	–
Poly (dG-dC)	3030±2	1740±32
Poly (dI-dC)	2610±22	1620±91

The binding isotherms for **APAC** with poly (dA-dT), poly (dA)-poly(dT), poly (dG-dC) and poly (dI-dC) are shown in Fig. 3b, the corresponding plots for **N-Et-AMAC** are linear (not shown) and the binding data are collected in Table 3. These data clearly indicate significant variations in the binding affinities of the probes as a function of the DNA sequence. The highest values are noted for poly(dA-dT) while the lowest value was observed for **APAC**/poly(dG-dC), as discussed below.

The binding constants of **APAC** with AT and GC sequences are quite distinct and are not within experimental error. The affinity of **APAC** for alternating AT sequences is 3.4 times higher than that of alternating GC sequences. The enhanced sequence recognition of **APAC** is attributed to the position of the ammonium group in the alkyl chain. The alkyl chain of **APAC** can fold onto itself to position the ammonium group close to the hydrogen bonding acceptor sites of the adjacent base pairs (Scheme 1B). Hydrogen bonding interactions between the ammonium group of **APAC** and the O2

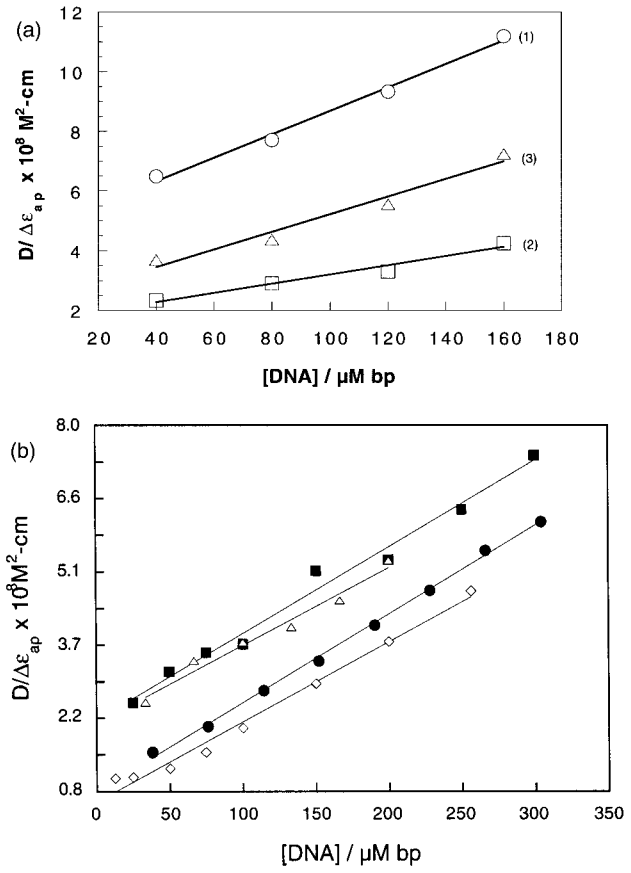

Figure 3. (a) Binding isotherms for **AMAC** (○, 37 μM), **APAC** (□, 20 μM), **N-Et-AMAC** (△, 21 μM) with CTDNA. The corresponding binding constants are estimated as $1.5\pm0.5\times10^4$, $1.4\pm0.1\times10^4$ and $1.2\pm0.1\times10^4\ M^{-1}$ (base pairs) for probes **AMAC**, **APAC**, and **N-Et-AMAC**, respectively. (b) Binding isotherms for **APAC** with poly(dA-dT) (◇), poly(dG-dC) (△), poly(dA)-poly(dT) (■), and poly(dI-dC) (●).

of thymine are most likely responsible for the enhanced sequence recognition. The presence of the 2-NH_2 group of guanine in the minor groove of G-C sequences sterically inhibits this hydrogen bonding interaction. If the 2-amino functionality of guanine is replaced by a hydrogen, as in the case of inosine, then the three dimensional arrangement of the hydrogen bonding groups in the minor groove of I-C sequences is similar to that of A-T sequences (Scheme 2).[17] As expected, the binding constants of **APAC** with poly(dA-dT) and poly(dI-dC) are similar within experimental error.

Further evidence for the importance of hydrogen bonding interactions between the probe and hydrogen bonding sites in the minor groove of DNA was obtained by comparing the binding constant of **N-Et-AMAC** with various DNA sequences. In contrast to **APAC**, **N-Et-AMAC** shows binding constants that are nearly independent of the DNA sequence, and the K_{AT}/K_{GC} is close to 1. The position of the amino functionality in the side chains of **APAC** and **N-Et-AMAC** is different while the steric factors associated with these side chains are identical. The affinity of **N-Et-AMAC** to all sequences examined are similar. This result suggests that the length of the spacer in **N-Et-AMAC** is not long enough to allow the ammonium group to be in close proximity with hydrogen bonding sites in the grooves of A-T sequences. Thus, the alkylammonium side chain plays a vital role in DNA sequence recognition. Based on these observations, the high affinity of **APAC** with alternating AT and IC sequences can be attributed to hydrogen bonding interactions of the ammonium group of **APAC** with the O2 of thymine (in AT sequences) or cytosine (in IC sequences).

Table 3. Strong dependence of binding constants of **APAC** and **N-Et-AMAC** on the DNA sequence. The binding constants are given in units M^{-1} of base pairs. The values in parentheses are the extinction coefficients of the free probes

DNA	**APAC** (7830)	**N-Et-AMAC** (4950)
CTDNA	$1.4\pm0.1\times10^4$	$1.2\pm0.1\times10^4$
Poly (dA-dT)	$3.0\pm0.6\times10^4$	$2.9\pm0.4\times10^4$
Poly (dA)-Poly(dT)	$1.1\pm0.2\times10^4$	–
Poly (dG-dC)	$8.9\pm0.2\times10^3$	$2.7\pm0.2\times10^4$
Poly (dI-dC)	$2.4\pm0.1\times10^4$	$2.4\pm0.3\times10^4$

Fluorescence spectra

The excited state properties of the anthryl probes are sensitive to their environment and their respective fluorescence spectra (1:40 probe to DNA ratio, excitation at 350 nm) are shown in Fig. 4. Extensively broad emission spectra are observed for **AMAC** and **N-Et-AMAC**, whereas no such broadening was observed with **APAC**. The emission spectra of the bound and the free forms are superimposable in case of **APAC** whereas those of **AMAC** and **N-Et-AMAC** are much broader for the bound species when compared to those of the free probes. No red shifts in the peak positions are apparent when these probes bind to DNA, in contrast to the corresponding absorption spectra.

The relative intensities of the 0–0 and the 0–2 vibrational bands of **AMAC** and **N-Et-AMAC** change upon binding to CTDNA, when the 0–1 band was used to normalize the spectra. The intensity of the 0–0 band decreases while the 0–2 band increases with increasing DNA concentration (data not shown). These changes are indicative of the subtle differences in the equilibrium geometries of the ground and excited vibronic states of the bound and free probes. No changes in the relative intensities of the vibrational bands of **APAC** are observed with increasing CTDNA concentration.

The fluorescence from the three anthryl probes is quenched by DNA, and the quenching efficiencies (K_{sv}) estimated from the Stern–Volmer quenching plots with CTDNA are $1.0\times10^4\ M^{-1}$ (**AMAC**), $1.4\times10^4\ M^{-1}$ (**APAC**), and $1.2\times10^4\ M^{-1}$ (**N-Et-AMAC**). The quenching cannot be due to energy transfer, as anthryl excited states are much lower in energy than the lowest excited states of the nucleobases.[18] An alternative to this mechanism is that quenching occurs via the electron transfer pathway and such quenching is expected to depend on DNA sequence. Among all the bases, the oxidation potential of guanine is the lowest.[19] The K_{sv} values for the quenching of **AMAC** fluorescence by poly(dG-dC), CTDNA, poly(dA-dT), and poly(dA)-poly(dT) are $1.2\times10^4\ M^{-1}$, $1.0\times10^4\ M^{-1}$, $7.4\times10^3\ M^{-1}$, and $2.1\times10^3\ M^{-1}$, respectively. Since **AMAC** binding does not depend on DNA sequence, the higher quenching

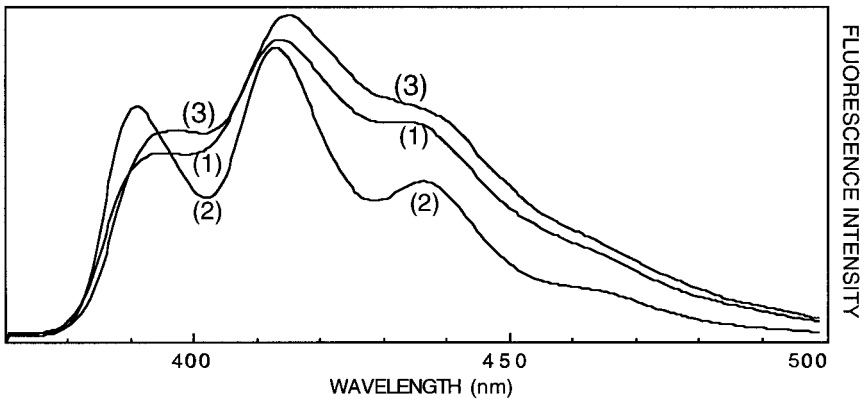

Figure 4. Fluorescence spectra of **AMAC** (1, 10 μM), **APAC** (2, 5.7 μM) and **N-Et-AMAC** (3, 4.9 μM) in the presence of CTDNA (1: 40 probe: DNA), with excitation at 350 nm. Broadening and red-shift are observed only with **AMAC** and **N-Et-AMAC**.

efficiency with poly(dG-dC) can be explained based on the lower redox potential of the guanine base.

Quenching studies with iodide

Accessibility of the DNA bound probes to the aqueous medium is investigated in quenching studies with iodide. Anionic quenchers can be used to distinguish between different DNA binding modes.[20,21] Intercalated chromophores (Scheme 3) are less accessible to quenching by iodide due to electrostatic repulsion between the negatively charged DNA and iodide. On the other hand, probes which are bound at the surface (groove binding or electrostatic binding) or free in solution are more accessible and therefore emission from these probes can be quenched more efficiently. The extent of protection offered by the DNA helix as estimated from the Stern–Volmer quenching slopes (K_{sv}) can indicate the relative exposure of the probes to the quencher. The quenching efficiencies as well as the relative decreases in the quenching constants in the presence and absence of DNA are collected in Table 4. All quenching plots are linear (Fig. 5, Fig. 6). and quenching constants are equal to the slopes of these plots. Emission from free probes is efficiently quenched by iodide, and quenching constants decrease substantially in the presence of CTDNA, indicating extensive protection of the chromophores by DNA. The degree of protection provided by CTDNA is in the order **AMAC** (23%)<**APAC** (31%)<**N-Et-AMAC** (47%).

The iodide quenching constants of the probes monitored in the presence of different DNA sequences show that the degree of protection is sequence dependent. The K_{sv} values for **APAC** and **N-Et-AMAC** in the presence and in the absence of various DNA sequences are listed in Table 4. The highest protection was offered by poly(dA-dT) whereas poly(dA)-poly(dT) provided the least protection (Fig. 5). The protection offered by poly(dG-dC) is clearly less than by CTDNA. These results can be correlated with the spectral data. First, the high iodide quenching efficiency observed with homo A-T polymers is consistent with the poor affinity or groove binding of these probes at this DNA sequence. Second, the decreasing extent of protection of **APAC** from iodide with increasing GC content of the DNA polymer is consistent with decreasing binding constants. Third, greater protection of **APAC** with poly(dA-dT) (K_{SV}=35 M^{-1}, 58% protection) than with poly(dG-dC) (K_{SV}=60 M^{-1}, 29% protection) is consistent with the greater affinity of **APAC** for alternating AT sequences than for GC sequences. The quenching constants with all DNA polymers, except poly(dG-dC), correlate inversely with the binding constants (Table 3).

Table 4. Fluorescence quenching constants (the estimated error in the K_{sv} values was ±2%) (M^{-1}), with iodide as the quencher, measured with 2 μM probe and 1:40 probe to DNA ratio. Emission was monitored at 413 nm for **APAC**, and 415 nm for **N-Et-AMAC** samples when excited at the corresponding isosbestic points. The values in parentheses correspond to the % protection from iodide quenching

DNA	**APAC**	**N-Et-AMAC**
No DNA	84	132
CTDNA	58 (31)	70 (47)
Poly(dA)-Poly(dT)	70 (17)	106 (20)
Poly (dG-dC)	60 (29)	109 (17)
Poly (dA-dT)	35 (58)	26 (80)
Poly (dI-dC)	56 (33)	73 (45)

Interpretation of the KI quenching data is complicated by the fact that different DNA sequences quench anthryl fluorescence to different extents and this leads to some disagreement between the iodide quenching results and the binding studies. For example, the binding constant of **APAC** is the lowest for poly(dG-dC), therefore, the quenching slope for this polymer is expected to be lower or similar to that of poly(dA)-poly(dT). The small difference in the quenching constant for these two DNA polymers is due to the fact that poly(dG-dC) quenches the fluorescence of **APAC** efficiently and the emission is predominantly from the free probe. The KI quenching data show that the order of protection of **N-Et-AMAC** is as follows: poly(dA-dT)>CTDNA>poly(dI-dC)>poly(dA)-poly(dT)> poly(dG-dC) while the binding constant data show that **N-Et-AMAC** binds to all DNA sequences with nearly equal affinity. The binding geometry and the binding mode are also key factors that influence these results, although, the binding modes are expected to be similar for these probes. No marked difference can be expected.

The difference between the protection offered by homo and hetero AT sequences is not surprising given the substantial

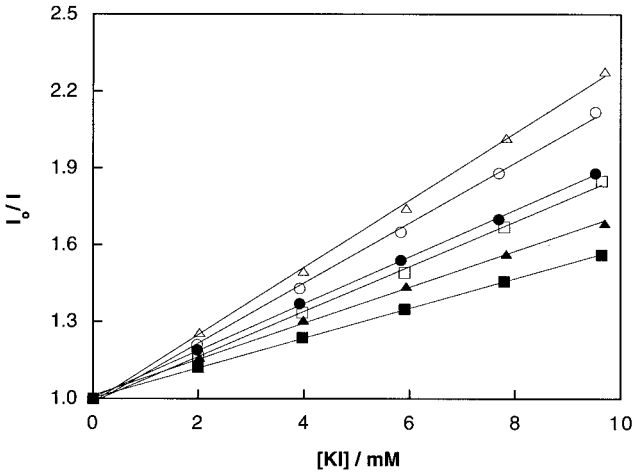

Figure 5. Stern–Volmer quenching plots of 2 μM **AMAC** (○), 2.4 μM **APAC** (□), and 2.4 μM **N-Et-AMAC** (△) in the presence of 60 μM (●), 80 μM (■), and 100 μM CTDNA (▲), respectively. **AMAC** was excited at 388 nm while **APAC** and **N-Et-AMAC** were excited at 390 nm. Emission was monitored at 410 for **AMAC**, 413 nm for **APAC**, and 415 nm for **N-Et-AMAC**.

differences in their helix structures. The homo AT sites are more flexible and show low affinities for intercalators.[22] In contrast, the quenching slope with poly(dG-dC) was in between the above polymers with a moderate affinity for the three probes. Thus, alternating AT sequences provide the best protection for the probe, indicating strong binding for these sequences. Such a strong sequence dependence with simple hydrophobic molecules is interesting, and indicates that hydrophobic binding of aromatics can be selective and provide a new avenue for the design of reagents to target specific segments of DNA helices.

Fluorescence lifetimes

The fluorescence lifetimes recorded with these probes provide further evidence for the interactions of these probes with DNA. The fluorescence lifetime of **APAC** in buffer is 8.4 ns and in the presence of CTDNA the fluorescence decay was a biexponential and the decay trace could be adequately fitted using lifetimes 1.8 ns (6%) and 8.9 ns (94%). The observation of the shorter lifetime (minor component) is a clear evidence for dynamic quenching of **APAC** emission by DNA. In contrast, the fluorescence lifetime of **N-Et-AMAC** changes from 11 ns to 10 ns (70%) and 21 ns (30%), in the presence of CTDNA. The shorter-lived component in both cases is due to emission from the site that is susceptible to quenching, and GC sequences are expected to quench the emission more efficiently than AT sequences.

Induced circular dichroism spectra

Interaction of an achiral molecule with a chiral environment can result in induced circular dichroism (ICD). The ICD of drugs or small molecules intercalated into DNA has been used to probe the orientation of the chromophore with respect to the base-pair dyad axis.[23] For instance, if the long axis of the intercalator is oriented parallel to the base pair long axis, a negative ICD is observed and positive ICD is reported for a perpendicular orientation. The ICD spectra of **AMAC**, **APAC** and **N-Et-AMAC** in the presence of calf thymus DNA (1:4 probe to DNA ratio) are shown in Fig. 7a. Positive ICD in the anthryl absorption region (320–420 nm) was observed for all the probes with CTDNA, and the peak positions of the ICD bands correspond to the red shifted absorption bands of the bound probe. The ICD peaks for **AMAC** are at 397, 377 and 357; for **APAC** at 396, 376 and 356; and for **N-Et-AMAC** at 396, 376 and 358 nm. The ICD spectra are better resolved for **APAC**, when compared to those of **AMAC** and **N-Et-AMAC**, consistent with the absorption spectra of the DNA-bound probes. These observations are also in agreement with the binding of **APAC** to a subset of sites, when compared to **AMAC** and **N-Et-AMAC**. The intensities of the ICD bands of **APAC** are greater than that of **AMAC** or **N-Et-AMAC** (300 μM CTDNA, 75 μM probe).

The ICD spectra of **APAC** with CTDNA, poly (dA-dT), and poly (dG-dC) (1:4 probe to DNA ratio) are shown in Fig. 7b. The ICD spectrum of **APAC** in the presence of poly(dA-dT) (curve 2) shows bands at 398, 376, and 355 nm and it is markedly red shifted when compared to that with CTDNA (curve 1). The spectrum obtained in the presence of

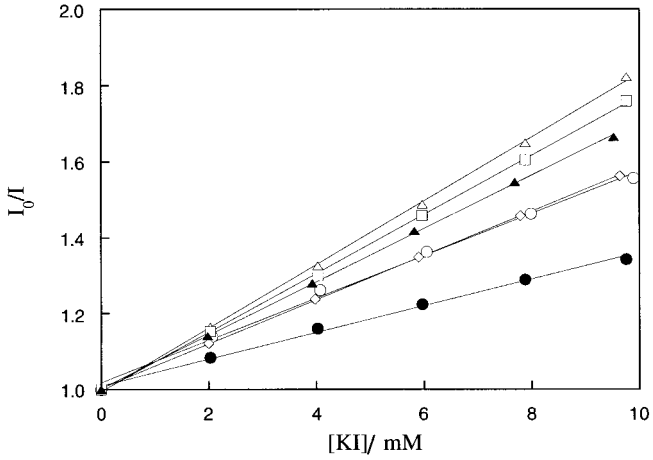

Figure 6. Sequence dependence of protection of **APAC** (2.4 μM) emission from iodide quenching. The data show the Stern–Volmer quenching plots for free probe (△), in the presence of 80 μM CTDNA (◇), 102 μM poly(dA-dT) (●), 96 μM poly(dG-dC) (□), 92 μM poly(dA)-poly(dT) (▲), and 96 μM poly(dI-dC) (○).

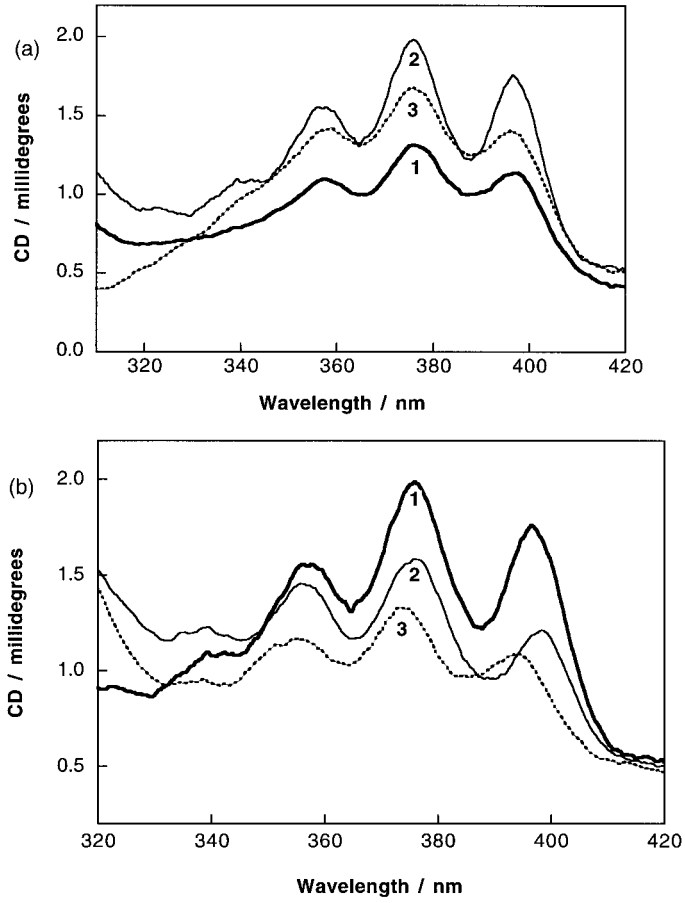

Figure 7. (a) CD spectra of **AMAC** (1, 75 μM), **APAC** (2, 74 μM), and **N-Et-AMAC** (3, 75 μM) in the presence of CTDNA (300 μM). In the absence of DNA, the probes have no CD and a flat baseline was observed. (b) CD spectra of **APAC** (75 μM) in the presence of CTDNA (1, 300 μM), poly (dA-dT) (2, 300 μM), and poly(dG-dC) (3, 300 μM).

poly(dG-dC), in contrast, is blue shifted (curve 3) when compared to that with CTDNA, with peaks at 394, 373, and 354 nm. The ICD bands are most intense with calf thymus DNA, and least intense with poly(dG-dC). The ICD bands are broader with poly(dG-dC) than with poly(dA-dT). In all cases, intercalation is a distinct possibility and positive ICD bands are observed, consistent with the orientation of the anthryl chromophore long axis perpendicular to the base pair dyad axis. This geometry appears to hold for all the three probes examined.

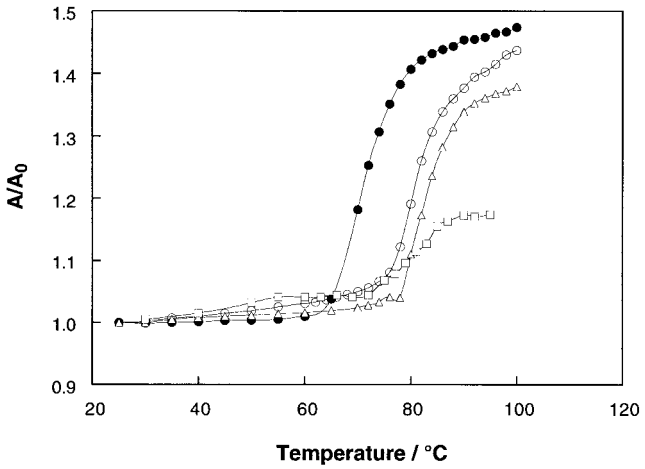

Figure 8. The helix melting curves for pure CTDNA (●, 60 μM) and in the presence of **AMAC** (□, 54 μM), **APAC** (○, 60 μM) and **N-Et-AMAC** (△, 60 μM) (pH 7.2, 5 mM Tris–HCl, 10 mM NaCl).

Helix melting studies

Intercalation of drugs or small molecules into DNA increases the helix melting temperature (T_m) indicating that intercalation can increase the stabilization of the double helix.[24] Helix melting is monitored by measuring the DNA absorbance at 270 nm as a function of temperature (Fig. 8). The absorbance increases sharply as the helix melts and the DNA strands separate. The DNA melting curves of calf thymus DNA in the presence, and in the absence of **AMAC**, **APAC** or **N-Et-AMAC** are presented in Fig. 8. The melting temperature of CTDNA increased from 70°C to 80, 80 and 82°C upon binding of **AMAC**, **APAC**, and **N-Et-AMAC**, respectively. Therefore, all the three probes stabilize the duplex with a considerable increase in T_m. The change in melting temperature (ΔT_m) of the three probes are similar to those reported for other intercalators.[33] The helix melting temperatures of poly(dA-dT) and poly(dG-dC) in the presence of our probes (Table 5) indicate intercalation of these probes into various helices. In case of poly(dG-dC), no melting was observed up to 93°C, the known T_m for this polymer and higher temperatures could not be examined.

Table 5. Helix melting temperatures (°C) for the probes **APAC** and **N-Et-AMAC** as a function of the DNA sequence. Higher melting temperatures were observed in the presence of the probes

DNA Sample	No probe	**APAC**	**N-Et-AMAC**
CTDNA	70	80	82
Poly(dA-dT)	57	69	69
Poly(dG-dC)	93	>93	>93

Thus, intercalation into the DNA samples is indicated by these data consistent with the spectral data outlined above.

Fluorescence polarization

Intercalation of the probes is further examined in fluorescence polarization studies. The rotational mobility of the probes is expected to decrease upon intercalation into the DNA helix and decreased mobility increases fluorescence polarization.[20,21] In the absence of DNA, negligible or no polarization was observed (Table 6). The fluorescence of **APAC**, on the other hand, was polarized in the presence of all DNA sequences except for poly(dG-dC). Highest polarization was observed in the presence of poly(dA-dT) and lowest polarization was observed in the presence of poly(dG-dC) clearly indicating the preferential binding at AT sites. Fluorescence from **N-Et-AMAC** was polarized in the presence of all DNA samples but the magnitude depended on the sequence. The fluorescence of **N-Et-AMAC** in the presence of poly(dA-dT) was highly polarized and less polarization was observed with poly(dG-dC), but this value is nearly 10 fold larger than that with **APAC**. Large increase in the fluorescence polarization in the presence of poly(dA-dT) suggests that both probes intercalate into these sequences. These data again suggest intercalation of the anthryl probes into various DNA sequences with **APAC** showing diminished intercalation into GC sites. Evidence is the strongest for intercalation into AT sites.

Sensitization of probe emission by DNA bases

Strong interactions observed in the absorption, and ICD spectra clearly indicate, when coupled with the melting and polarization studies, intercalation of the probes into the helix. We have used nucleobase sensitized fluorescence from anthryl probes as a sensitive method to test for intercalation.[8,20a,12] Singlet state energies of all the bases are larger than that of the anthryl chromophore[29] and exothermic energy transfer from DNA to anthryl probes is expected (Scheme 4). The DNA emission bands overlap with the anthryl absorption bands and this fact further increases the energy transfer probability from DNA to the

Table 6. Fluorescence polarization values of **APAC** and **N-Et-AMAC** in the presence and in the absence of various DNA sequences. Excitation was at 390 nm and the emission was monitored at 415 nm (1:40 probe to DNA concentration ratio, 2 μM probe)

DNA	**APAC**	**N-Et-AMAC**
No DNA	0.000±0.002	−0.004±0.003
Calf thymus DNA	0.011±0.003	0.020±0.003
Poly(dA)-Poly(dT)	0.018±0.005	0.030±0.003
Poly (dG-dC)	0.001±0.003	0.012±0.003
Poly (dA-dT)	0.056±0.007	0.089±0.005
Poly (dI-dC)	0.014±0.002	0.043±0.006

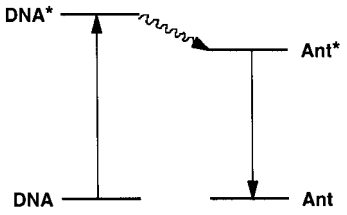

Scheme 4. Energy transfer scheme illustrating the sensitization of probe emission by the DNA bases.

anthryl probes. Energy transfer is used here as another tool to examine the binding of these molecules into the DNA helix. DNA bases sensitize the anthryl fluorescence from **APAC** and **N-Et-AMAC**, upon excitation in the 260–300 nm region. Energy transfer was monitored by recording the fluorescence spectra while exciting into the DNA absorption bands (Scheme 4). Efficient energy transfer to the anthryl chromophore was observed (spectra not shown), consistent with the intercalation of the probes into the helix. When the helix was melted at 90°C, no energy transfer was observed to any of the probes and the emission spectrum returns to that of the free chromophore. Energy transfer from DNA was confirmed by recording the excitation spectra of the probes in the presence and in the absence of DNA (Fig. 9a and b). Pure DNA solutions showed no excitation bands in the 250–300 nm region when the emission was monitored at >400 nm. The excitation spectra of the free probes match with their respective absorption spectra in 250–400 nm region. However, in the presence of DNA containing AT sequences, the excitation spectra show an additional band in the 270–300 nm region (Fig. 9a and b), absent in the free anthryl chromophore. No such excitation bands are observed with poly(dG-dC) and this is partly due to the strong quenching of anthryl excited states by GC sequences or that GC sites do not transfer energy. Such sequence dependent energy transfer from **AMAC** and **N-Et-AMAC** has been reported previously.[8,20a,12] Helix structure and intercalation of the chromophore are essential for the observed energy transfer.

DNA photocleavage

DNA binding properties can be utilized to photocleave the DNA polymer. Excitation of the anthryl probes in the near UV region results in efficient photocleavage of the DNA backbone (Fig. 10A and B). Photocleavage of supercoiled pBR322 DNA by **APAC**, and **N-Et-AMAC** resulted in efficient conversion of supercoiled DNA (form I) to the nicked circular DNA (form II). The linear DNA (form III) was obtained by treating supercoiled pBR322 with EcoRI (lane 1). Only very faint bands corresponding to the linear DNA could be identified in lanes 2–9, and the product is mostly form II DNA (lanes 4–9). The photocleavage of pBR322 by these probes proceeds rapidly, indicating the photoreactivity of the anthryl chromophore. The photocleavage data, although preliminary, clearly establishes that these anthryl probes cleave DNA under photochemical conditions. Sequence dependent photocleavage of DNA by **AMAC** has been previously reported,[9] and future studies will provide further details about how the excited states of these probes interact with DNA as a function of sequence.

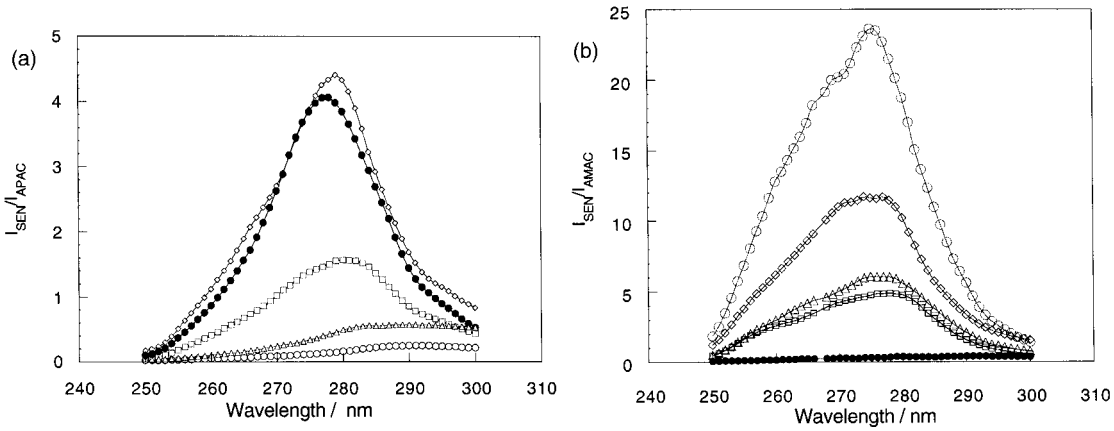

Figure 9. (a) Ratio of fluorescence intensity of **APAC** in the presence of: (1) poly(dA)-poly(dT), ◇; (2) poly(dA-dT), ●; (3) CTDNA, □; (4) poly(dG-dC), △; (5) poly(dI-dC), ○, to the fluorescence intensity of **APAC** in the absence of DNA. Solutions contain 1:40 probe to DNA ratio and the emission was monitored at 438 nm. No energy transfer was observed with poly(dG-dC) and poly(dI-dC). (b) Ratio of the fluorescence intensity of **N-Et-AMAC** in the presence of: (1) poly(dA-dT), ○; (2) poly(dA)-poly(dT), ◇; (3) CTDNA, △; (4) poly (dI-dC), □; (5) poly (dG-dC), ●, to the fluorescence intensity of **N-Et-AMAC** in the absence of DNA. Solutions contain 1: 40 probe to DNA ratio and the emission was monitored at 438 nm. No energy transfer was observed with poly(dG-dC).

Conclusions

The length of the linker and the cationic ammonium group of **APAC/N-Et-AMAC** play significant roles in the binding to the DNA helix. This perhaps indicates the proximity of the amine function to the negatively charged phosphate groups or hydrogen bonding sites on the helix. Fluorescence polarization measurements, energy transfer, and CD data clearly show intercalation into the helix. **APAC** intercalates into alternating AT and IC sequences while discriminating against GC sequences. The CD, helix melting, and energy transfer studies are consistent with the binding studies. While energy transfer from the DNA to the probe requires intercalation, the converse is not necessarily true. The binding mode proposed for **APAC** is consistent with its higher affinity for both AT and IC sequences. The geometrical isomer, **N-Et-AMAC**, differs in its DNA binding properties due to the position of ammonium group in the side chain. The probes intercalate into the helix and the side chain is important in the sequence/base recognition. Such a simple recognition element may be useful in future designs.

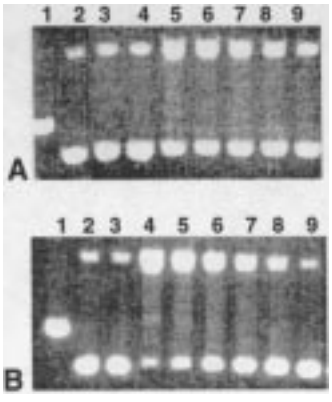

Figure 10. DNA photocleavage by anthryl probes. Irradiation times are linearly correlated with the production of nicked circular DNA. In each gel, linear DNA (pBR322 treated with EcoRI) was loaded in lane 1 for comparison. Lanes 2 and 3 contained pBR322 irradiated for 120 and 60 min. In A, lanes 4, 5, 6, 7, 8 and 9 contain DNA and **APAC** irradiated at 390 nm for 0, 120, 90, 60, 40 and 20 min, respectively. In B, Lanes 4, 5, 6, 7, 8 and 9 correspond to DNA and **N-Et-AMAC** mixtures irradiated for 120, 90, 60, 40, 20, and 0 min, respectively.

Current results clearly indicate that it is possible to design molecular systems that can bind to selected sites with preponderance over the other sites. The linker connecting the aromatic chromophore and the cationic function is important in dictating the binding interactions as well as the photophysical properties of the bound probe. Such selectivity may be exploited in future experiments for better discrimination between different DNA sequences. Higher affinity of **APAC** for AT sequences indicates that planar aromatics can be used to display specific hydrogen bonding groups in the grooves of the double helix for sequence recognition. Intercalation provides a reference frame to position the hydrogen bonding functions at desired locations.

Experimental

The DNA samples were purchased from Sigma Chemical Co. Calf thymus DNA, form I, was purified by phenol extraction as described in the literature.[25] Purity of the final DNA preparation was checked by monitoring its absorption spectrum, and from the ratio of absorbance at 260–280 nm. The synthetic deoxyribonucleotides are used as received, without further purification. All samples were dissolved in 5 mM Tris buffer, pH 7.2, 50 mM NaCl, unless mentioned otherwise. DNA concentrations per nucleotide were determined by absorption spectroscopy, using the following molar extinction coefficients ($M^{-1}\,cm^{-1}$) at the indicated wavelengths: calf thymus DNA, 6600, 260 nm; poly(dA-dT), 6600, 260 nm; poly(dA)-poly(dT), 6000, 260 nm; poly(dG-dC), 8400, 254 nm; and poly(dI-dC), 6900 at 251 nm.[26]

Synthesis and characterization of 9-anthrylmethylammonium chloride (**AMAC**) was previously reported.[20] 3-(9-Anthryl)-propylammonium chloride (**APAC**) was prepared by reacting 9-anthraldehyde with cyanoacetic acid.[27] The resulting

acrylonitrile derivative was reduced first with sodium borohydride by following a reported method,[28] and then with lithium aluminum hydride[29] to obtain the primary amine in 81% yield. The amine was converted to the hydrochloride salt by treating with dilute hydrochloric acid. Solvent was evaporated under vacuum, the residue was dissolved in methanol and recrystallized from ether: yield 81%; mp 242–244°C dec; ^{1}H NMR (Bruker 270 MHz, DMSO-d_6) δ 8.49 (s, 1H), 8.37 (d, J=8 Hz, 2H), 8.07 (t, J=8, 2 Hz, 5H), 7.54 (m, 4H), 3.68 (t, J=8 Hz, 2H), 3.03 (br s, 2H), 1.98 (m, 2H); MS (EI) *m/e* (relative intensity) 235 (M^+-HCl, 20), 217 (29), 203 (44), 191 (72), 178 (54), 56 (100), 36 (34), 28 (42). *N*-Ethyl-(9-anthryl)methylammonium chloride (**N-Et-AMAC**) was prepared following a reported procedure.[30] Yield 95%; mp 218–220°C dec; ^{1}H NMR ($CDCl_3$) δ 9.93 (br s, 2H), 8.49 (s, 1H), 8.35 (d, J=9 Hz, 2H), 7.97 (d, J=8 Hz, 2H), 7.68 (t, J=7, 9 Hz, 2H), 7.50 (t, J=7 Hz, 2H), 5.02 (s, 2H), 2.75 (s, 2H), 1.26 (t, J=7 Hz, 3H); MS (EI) *m/e* (relative intensity) 235 (M^+-HCl, 73), 204 (57), 191 (100), 178 (82), 165 (50), 56 (68), 44 (53), 36 (59), 28 (56).

All the absorption spectra were recorded on a Perkin–Elmer Lambda 3B spectrophotometer and all the fluorescence spectra were recorded on a Perkin–Elmer LS5B spectrometer. Both spectrometers were interfaced with an Apple Macintosh computer and all the necessary software to control the spectrometers was developed in our laboratory. The absorption and the fluorescence titrations were performed by keeping the concentration of the probe constant while varying the nucleic acid concentration. This was done by mixing various proportions of the probe and the DNA stock solutions while maintaining the total volume of the mixture constant (1 mL). In fluorescence measurements, the air-saturated solutions were excited at the corresponding isosbestic points and the fluorescence intensity was monitored as a function of wavelength.

The intrinsic binding constants of the probes with calf thymus DNA and with synthetic DNA samples were determined in absorption and fluorescence titrations. In absorption titrations, the absorbance at 365 nm was recorded after each addition of DNA, and the intrinsic binding constant K was determined from the plot of $D/\Delta\epsilon_{ap}$ vs. D using Eq. (1),[31] where D is

$$\frac{D}{\Delta\epsilon_{ap}} = \frac{D}{\Delta\epsilon} + \frac{1}{\Delta\epsilon K} \quad (1)$$

the concentration of DNA in base pairs, $\Delta\epsilon_{ap}=[\epsilon_a-\epsilon_F]$ and $\Delta\epsilon=[\epsilon_B-\epsilon_F]$. The apparent extinction coefficient, ϵ_a, is the ratio of the observed absorbance of the sample (A_{obsd}) and the total concentration of the probe. ϵ_B and ϵ_F correspond to the extinction coefficients of the bound and free probe, respectively. ϵ_B was independently determined from a plot of the absorbance at 365 nm vs. 1/[DNA], and the y-intercept is equal to the absorbance at infinite concentration of DNA. The data are analyzed using Eq. (1), where the intrinsic binding constant (K) is equal to the ratio of the slope ($1/\Delta\epsilon$) to the y-intercept ($1/\Delta\epsilon K$). K is calculated from the best fits of the data using Eq. (1).

In fluorescence quenching experiments, the data are plotted according to the Stern–Volmer Eq. (2)[32] where I_0 and I are the fluorescence intensities in the absence and in the presence of the quencher. K_{SV} is the Stern–Volmer quenching constant which is a measure of

$$\frac{I_0}{I} = 1 + K_{SV}[Q] \quad (2)$$

the efficiency of quenching, and [Q] is the quencher concentration. Probes bound to DNA are protected from anionic quenchers such as iodide and the quenching experiments provide a simple method to distinguish between the bound and free chromophores.[21]

The DNA melting studies were conducted with a Hewlett–Packard 8452A diode array spectrophotometer equipped with an HP 89090A peltier thermostat, controlled by an HP Vectra 386/16N computer. The DNA melting experiments with probes **APAC** and **N-Et-AMAC** were monitored at 270 nm due to the strong absorption of these probes at 260 nm. From this data, the DNA absorbance at 270 nm was plotted as a function of temperature to obtain the helix melting temperatures.

Fluorescence lifetimes and time-resolved fluorescence spectra were recorded on a home-built single photon counting spectrometer, as described earlier.[33] The software necessary for the collection and manipulation of the data was developed in our laboratory. The fluorescence decay profiles were deconvoluted with software from PRA Inc. and the goodness of fits was tested from various parameters such as χ^2, Durbin–Watson parameter, and the correlation function.

The fluorescence polarization measurements were carried out on a Perkin–Elmer LS-50 spectrometer. In these measurements, the ratio of probe to DNA phosphate concentration was kept at 1:40 to ensure complete binding of the probe. The samples were excited at the isosbestic point and the fluorescence signal was monitored at 415 nm, through crossed polarizers.

The CD spectra were recorded on a Jasco-710 spectropolarimeter. A quartz microcell (10 mm pathlength) was used for these measurements. The operating parameters were, bandwidth 1 nm, sensitivity 20 millidegrees, and response time 4 s. The DNA concentration was kept constant at 300 μM and increasing volumes of the probe-DNA mixtures were added until the ratio of probe to DNA concentrations was 0.25.

The photocleavage studies were done by exposing the samples to 390 nm radiation from a 150 W PTI Model LPS-220 light source attached to a quarter meter monochromator. The power supply was operated at 130W and the intensity of the light beam remained constant within ±5%, on a day-to-day basis. The sample tubes were placed horizontally in the light path for irradiation and the reaction mixture (total volume, 48 μL) consisted of 10 μM of DNA (in base pairs) dissolved in Tris buffer. Aliquots of 8 μL samples were withdrawn after irradiation for 0, 15, 30, 60, 90 and 120 min. To check for light damage, dark and light controls (for 2 h) were maintained, under similar conditions. The DNA samples were loaded onto a 1% agarose gel and

have been electrophoresed at 100 V for 70 min. using the running buffer consisting of 1 M Tris base, 1 M boric acid, and 0.02 M Na_2EDTA (pH 8). After the electrophoresis, the gel was stained with ethidium bromide, and has been destained with water. The photographs of gels were scanned and digitized using ADOBE PHOTOSHOP Software v. 2.5.1. NIH Image software was used to convert the images into gel-electrophoretograms. Peaks corresponding to form I and form II DNA were integrated and plotted as a function of time.

References

1. Neidle, S.; Waring, M., Eds.; *Molecular Aspects of Anticancer Drug-DNA Interactions*; CRC: Boca Raton, 1993; Vols. 1 and 2; D'incalci, M.; Sessa, C. *Expert Opin. Invest. Drugs* **1997**, *6*, 875.
2. Kimura, E.; Ikeda, T.; Shionoya, M., *Pure Appl. Chem.* **1997**, *69*, 2187; Wemmer, D. E.; Dervan, P. B. *Curr. Opin. Struct. Biol.* **1997**, *7*, 355; Trauger, J. W.; Baird, E. E.; Dervan, P. B. *Nature* **1997**, *382*, 559.
3. Mestre, B.; Jakobs, A.; Pratviel, G.; Meunier, B. *Biochemistry* **1996**, *35*, 9140; Kahne, D. *Chem. Biol.* **1995**, *2*, 7; Arrowsmith, J.; Missailidis, S.; Stevens, M. F. G. *Anti-Cancer Drug Des.* **1999**, *14*, 205; Long, E. C. *Acc. Chem. Res.* **1999**, *32*, 827; Sardesai, N. Y.; Barton, J. K. *J. Biol. Inorg. Chem.* **1997**, *2*, 762; Takenaka, S.; Iwamasa, K.; Takagi, M.; Nishino, N.; Mihara, H.; Fujimoto, T. *J. Heterocycl. Chem.* **1996**, *33*, 2043; Gatto, B.; Zagotto, G.; Sissi, C.; Cera, C.; Uriarte, E.; Palu, G.; Capranico, G.; Palumbo, M. *J. Med. Chem.* **1996**, *39*, 3114; Sardesai, N. Y.; Zimmermann, K.; Barton, J. K. *J. Am. Chem. Soc.* **1994**, *116*, 7502; Bailly, F.; Bailly, C.; Waring, M. J.; Henichart, J. P. *Biochem. Biophys. Res. Commun.* **1996**, *184*, 930.
4. Bailly, C.; Riou, J.-F.; Colson, P.; Houssier, C.; Rodrigues-Pereira, E.; Prudhomme, M. *Biochemistry* **1997**, *36*, 3917; Arcamone, F. *Gene* **1997**, *149*, 57.
5. Gewirtz, D. A. *Biochem. Pharmacol.* **1999**, *57*, 727; Walker, W. L.; Kopka, M. L.; Goodsell, D. S. *Biopolymers* **1998**, *44*, 323; Leng, F.; Priebe, W.; Chaires, J. B. *Biochemistry* **1998**, *37*, 1743; Bailly, C.; Kenani, A.; Waring, M. J. *Nucleic Acids Res.* **1997**, *25*, 1516; Bailly, C.; Brana, M.; Waring, M. J. *Eur. J. Biochem.* **1996**, *240*, 195; Sugiura, Y.; Kusakabe, T. *NATO ASI Ser. C* **1996**, *479*, 65.
6. Pastor, J.; Siro, J. G.; Garcia-Navio, J. L.; Vaquero, J. J.; Alvarez-Builla, J.; Gago, F.; de Pascual-Teresa, B.; Pastor, M.; Rodrigo, M. M. *J. Org. Chem.* **1997**, *62*, 5476; Fairley, T.; Molock, F.; Boykin, D. W.; Wilson, W. D. *Biopolymers* **1988**, *27*, 1433.
7. Terbrueggen, R. H.; Johann, T. W.; Barton, J. K. *Inorg. Chem.* **1998**, *37*, 6874; Wemmer, D. *Nat. Struct. Biol.* **1998**, *5*, 169.
8. Kumar, C. V.; Asuncion, E. H. *J. Chem. Soc., Chem. Commun.* **1992**, 470.
9. Kumar, C. V.; Tan, W. B.; Betts, P. W. *J. Inorg. Biochem.* **1997**, *66*, 177.
10. Al Rabaa, A. R.; Tfibel, F.; Merola, F.; Pernot, P.; Fontaine-Aupart, M.-P. *J. Chem. Soc., Perkin Trans. 2* **1999**, 341.
11. Wilson, W. D.; Wang, Y. H.; Kusuma, S.; Chandrasekaran, S.; Yang, N. C.; Boykin, D. W. *J. Am. Chem. Soc.* **1985**, *107*, 4989; Becker, H.-C.; Norden, B. *J. Am Chem. Soc.* **1999**, *121*, 11947.
12. Kumar, C. V.; Asuncion, E. H. *Chem. Commun.* **1999**, 1219.
13. Long, E. C.; Barton, J. K. *Acc. Chem. Res.* **1990**, *23*, 271; Dougherty, G.; Prigram, W. J. *Crit. Rev. Biochem.* **1982**, *12*, 103; Berman, H. M.; Young, P. R. *Annu. Rev. Biophys. Bioengng* **1981**, *10*, 87.
14. Cantor, C.; Schimmel, P. R. *Biophysical Chemistry*, W. H. Freeman: San Francisco, 1980 (Vol. 2, p 398).
15. Absorption and fluorescence titrations with a polyanion such as poly(sodium 4-styrenesulfonate) or with anionic micelles of sodium dodecyl sulfate did not show the changes observed with DNA; Asuncion, E. H. Ph.D. Thesis, University of Connecticut, 1994.
16. Ostaszewski, R.; Wilczynska, E.; Wolszczak, M. *Bioorg. Med. Chem. Lett.* **1998**, *8*, 2995; Schelhorn, T.; Kretz, S.; Zimmermann, H. W. *Cell. Mol. Biol.* **1992**, *38*, 345; Schmechel, D. E. V.; Crothers, D. M. *Biopolymers* **1971**, *10*, 465; LePecq, J.-B.; Paoletti, C. *J. Mol. Biol.* **1967**, *27*, 87.
17. Fabriciova, G.; Miskovsky, P.; Jancura, D.; Kocisova, E.; Lisy, V. *Gen. Physiol. Biophys.* **1995**, *14*, 203; Dasgupta, D.; Goldberg, I. H. *Nucl. Acids Res.* **1986**, *14*, 1089; Kearns, D. R.; Mirau, P. A.; Assa-Munt, N.; Behling, R. W. *Jerusalem Symp. Quantum Chem. Biochem.* **1983**, *16*, 113.
18. Eisinger, J. *J. Photochem. Photobiol.* **1968**, *7*, 597; Bishop, S. M.; Malone, M.; Phillips, D. *J. Chem. Soc., Chem. Commun.,* **1994**, 871.
19. Saito, I.; Takayama, M.; Sugiyama, H.; Nakatani, K. *J. Am. Chem. Soc.* **1995**, *117*, 6406; Sugiyama, H.; Saito, I. *J. Am. Chem. Soc.* **1996**, *118*, 7063.
20. (a) Kumar, C. V.; Asuncion, E. H. *J. Am. Chem. Soc.* **1993**, *115*, 8547. (b) Bottini, A. T.; Dev, V.; Klinck. *J. Organic Syntheses*; Wiley: New York, 1973; Collect Vol. V, p 121.
21. Kumar, C. V.; Barton, J. K.; Turro, N. J. *J. Am. Chem. Soc.* **1985**, *107*, 5518.
22. Wheeler, G. V.; Chinsky, L.; Miskovsky, P.; Turpin, P.-Y. *J. Biomol. Struct. Dyn.* **1995**, *13*, 399; Pilch, D. S.; Kirolos, M. A.; Liu, X.; Plum, G. E.; Breslauer, K. J. *Biochemistry* **1995**, *34*, 9962; Geacintov, N. E.; Shahbaz, M.; Ibanez, V.; Moussaoui, K.; Harvey, R. G. *Biochemistry* **1988**, *27*, 8380.
23. Becker, H.-C.; Norden, B. *J. Am. Chem. Soc.* **1997**, *119*, 5798; Monnot, M.; Mauffret, O.; Lescot, E.; Fermandjian, S. *Eur. J. Biochem.* **1992**, *204*, 1035; Norden, B.; Kubista, M. *NATO ASI Ser. C* **1988**, *242*, 133; Lyng, R.; Hard, T.; Norden, B. *Biopolymers* **1987**, *26*, 1327; Norden, B.; Tjerneld, F. *Biopolymers* **1982**, *21*, 1713; Schipper, P. E.; Norden, B.; Tjerneld, F. *Chem. Phys. Lett.* **1980**, *70*, 17.
24. Bhattacharya, S.; Thomas, M. *J. Indian Chem. Soc.* **1998**, *75*, 716; Remers, W. A.; Dorr, R. T.; Sami, S. M.; Alberts, D. S.; Bear, S.; Mayr, C. A.; Solyom, A. M. *Curr. Top. Med. Chem.* **1997**, *2*, 45; Cao, Y.; He, X.-W. *Spectrochim. Acta* **1998**, *54A*, 883; Cusumano, M.; Giannetto, A. *J. Inorg. Biochem.* **1997**, *65*, 137; Sobell, H. M.; Sarma, R. H., Eds.; *Nucleic Acid Geom. Dyn*; Pergamon, Elmsford: NY; p 289; Patel, D. J. *Acc. Chem. Res.* **1979**, *12*, 118; Patel, D. J.; Canuel, L. L. *Proc. Natl. Acad. Sci. USA*, **1996** *73*, 3343; Berman, H. M.; Young, P. B. *Annu. Rev. Biophys. Bioengng* **1981**, *10*, 87.
25. Maniatis, T.; Fritsch, E. F.; Sambrook, J. *Molecular Cloning: A Laboratory Manual*; Cold Spring Harbor Laboratory: New York; 1982; p 458.
26. Barton, J. K.; Goldberg, J. M.; Kumar, C. V.; Turro, N. J. *J. Am. Chem. Soc.* **1986**, *108*, 2081; Baguley, B. C.; Falkenhaug, E.-M. *Nucl. Acids Res.* **1978**, *5*, 161.
27. Hann, R. A. *J. Chem. Soc. Perkin Trans. 1* **1974**, 1379.
28. Rhodes, R. A.; Boykin, D. W. *Synth. Comm.* **1988**, *18*, 681.
29. Amundsen, L. H.; Nelson, L. S. *J. Am. Chem. Soc.* **1951**, *73*, 242.
30. Hutton, R. C.; Salam, S. A.; Stephen, W. I. *J. Chem. Soc. A* **1966**, 1573.

31. Pyle, A. M.; Rehmann, J. P.; Meshoyrer, R.; Kumar, C. V.; Turro, N. J.; Barton, J. K. *J. Am. Chem. Soc.* **1989**, *111*, 3051; Wolfe, A.; Shimer, G. H., Jr.; Meehan, T. *Biochemistry* **1987**, *26*, 6392.

32. Turro, N. J. *Modern Molecular Photochemistry*, Benjamin Cummings: Menlo Park, 1978 (p 305).

33. Kumar, C. V.; Williams, Z. J.; Turner, R. S. *J. Phys. Chem.* **1998**, *102*, 5562.